Exploring optoretinographic responses of photoreceptor function in disease-affected retinas

Reddikumar Maddipatla[a,b], Christopher S. Langlo[a], Kari V. Vienola[c], Maciej M. Bartuzel[a,b], Ewelina Pijewska[a,b,d], Robert J. Zawadzki[a,b], and Ravi S. Jonnal[a]

[a]Center for Human Ophthalmic Imaging Research (CHOIR), Dept. of Ophthalmology and Vision Science, UC Davis Eye Center, Sacramento, CA 95817, USA
[b]EyePOD Imaging Lab, Dept. of Cell Biology and Human Anatomy, UC Davis, Davis, CA 95616, USA
[c]Institute of Biomedicine, University of Turku, Turku, Finland
[d]Faculty of Physics, Astronomy, and Informatics, Nicolaus Copernicus University in Torun, Grudziądzka 5, 87-100 Torun, Poland

ABSTRACT

Assessment of the functional response of photoreceptors plays an important role in assessing and treating vision loss. Optoretinography (ORG) is an emerging non-invasive technique that measures the photoreceptors' functional response to external light stimuli using optical coherence tomography (OCT) or other phase-sensitive imaging modalities. Recently a novel velocity-based ORG method was demonstrated, illustrating the feasibility of measuring photoreceptor function with clinical-grade OCT systems. Here we test this technique on disease-affected retinae of human subjects. The disease-affected retinae exhibited altered responses when compared to a healthy volunteer. The findings indicate promise for this novel tool to find applications in the clinic and clinical research.

Keywords: optical coherence tomography, optoretinography, functional imaging, phase imaging, photoreceptors

1. INTRODUCTION

In blinding retinal diseases such as age-related macular degeneration (AMD) and retinitis pigmentosa (RP), dysfunction of photoreceptors is thought to precede their outright loss. Currently, in ophthalmic clinics, these diseases are detected and assessed by observing structural anomalies of the retinal layers using optical coherence tomography (OCT), normally in combination with subjective tests such as visual acuity (VA) and visual fields (VF). An ideal complement to these techniques would be an objective functional test based on imaging of the photoreceptors, which would reveal functional and structural changes simultaneously. Objective assessment of the functional response could greatly help ophthalmologists detect retinal diseases at an early stage and manage them effectively. It could also catalyze trials of therapeutics by supplying them with earlier and more sensitive endpoints.

OCT is a non-invasive, high-resolution, volumetric imaging technique commonly used to assess retinal layer abnormalities. In OCT the amplitude and phase of the light reflected by the sample are recorded, and usually the amplitude of the signal is used to generate high-resolution structural images of the sample, while the phase is ignored. By utilizing the phase of the OCT signal, nanometer-scale changes in the sample can be quantified,[1] which offers the ability to measure subtle structural changes in the photoreceptors due to external light stimuli.

Early efforts to observe these stimulus-evoked responses in human cone photoreceptors used adaptive optics (AO), enabling resolution and tracking of single cells, in conjunction with common path interferometry.[2] Since then, interest in this area has grown, and these responses have been successfully measured in single cones[3–8] and

Further author information: (Send correspondence to R.M.)
R.M.: E-mail: rkmaddipatla@ucdavis.edu

Ophthalmic Technologies XXXIV, edited by Daniel X. Hammer, Kostadinka Bizheva, Georg Schuele, Proc. of SPIE Vol. 12824, 1282406 · © 2024 SPIE
1605-7422 · doi: 10.1117/12.3003007

rods[9] using advanced OCT systems with cellular resolution achieved with adaptive optics (AO) or digital aberration correction (DAC). These approaches measure responses from single cells, most commonly by monitoring the phase difference between outer segment (OS) tips of cones (COST) or rods (ROST) and the inner-outer segment junction (IS/OS), and this approach has been termed optoretinography (ORG).

AO enables cellular ORG measurements because it permits the tracking of single cells over time. In this way, the "purest" responses are recorded, i.e., those without artifacts due to extracellular factors. It also permits complementary analysis of cell properties and structure both in health and disease.[5,10] The AO-ORG systems published thus far have been extremely fast, capitalizing on full-field OCT,[3] megahertz+ swept sources,[4,9] spectrometer multiplexing,[5] or line-illumination with 2D detection.[6] By being fast they were able to achieve both cellular resolution and the necessary temporal resolution to detect what we believe to be the main features of the photoreceptor ORG response. However, measuring ORG signals with an advanced AO system poses some challenges for clinical translation. Research-grade AO-OCT systems are costly and typically require multiple expert operators. The volume of processed data can be in the terabytes for a single experiment, requiring costly storage and backup systems, as well as protracted data processing times.

While most recent work in this area has utilized AO, earlier work showed that the amplitude of the OCT signal could be used to measure light-evoked changes in the retinae of animal models[11–13] and humans.[14] A challenge posed by clinical-grade OCT instrumentation is its relatively low speed. To measure the fastest ORG dynamics, sampling rates should be over 100 Hz, a volumetric imaging frequency afforded only by the uncommon high-speed OCT implementations listed above. Typical research-grade OCT implementations and clinical OCT systems cannot achieve volume rates this high, but can generally achieve sufficient B-scan rates. However, implementing the ORG with serial B-scanning requires a paradigm shift from the AO-ORG, since in awake humans the retina cannot be expected to be stationary for the duration of measurement. Thus, over the course of measurement, different parts of the retina are imaged. In the AO-ORG paradigm the phase of light reflected by structures is monitored over time, as those structures are tracked. In the absence of tracking, the structures in view vary over time. If this paradigm were applied to serial B-scans, microscopic axial variations in the structures being imaged, as they moved in and out of the scanning beam, would result in spurious phase changes mistaken for ORG signal.

We recently published results from a novel ORG paradigm designed for an OCT platform very similar to those used in clinics.[15] The method works by computing the relative velocities of the IS/OS and COST over a brief (5 ms to 10 ms) finite window, and rolling that window over the series of B-scans acquired over much longer durations. It also requires that the stimulus flash is delivered to all of the retina that moves into view during the longer interval. The key assumptions of this paradigm are 1) that photoreceptors that are near one another exhibit correlated ORG responses; 2) there is a finite interval over which eye movements are negligible compared to the spot size of the OCT; and 3) changes in the *rate* of OS length change are interchangeable with changes in the OS length. In the present work, we explore this method's ability to measure deficits in photoreceptor function in patients with vision loss.

2. METHODS

2.1 Imaging system

The OCT system is illustrated in Fig. 1. In short, it consists of a 1060 nm swept-source with a 100 kHz A-scan rate and 100 nm bandwidth (Axsun), two galvanometric scanners (Cambridge), a transmissive reference arm, balanced photoreceiver (Thorlabs), and digitizer (Alazar). A 90/10 fiber coupler sends 90% of the light to the reference arm and 10% to the eye. The backscattered light from the eye was combined with the reference light using a 50/50 fiber coupler, and a retroreflector was translated in one dimension to adjust the reference arm length. The optical power for the OCT in the sample arm at the pupil plane was measured to be 1.8 mW. The stimulus channel consists of a 555 nm LED to equally stimulate L and M cones. In the present experiment the stimulus was a 30 ms, 44 µW, circular flash subtending 1.2°. This flash isomerizes approximately 65 % of L and M photopigment in the stimulated region of a dark-adapted eye.

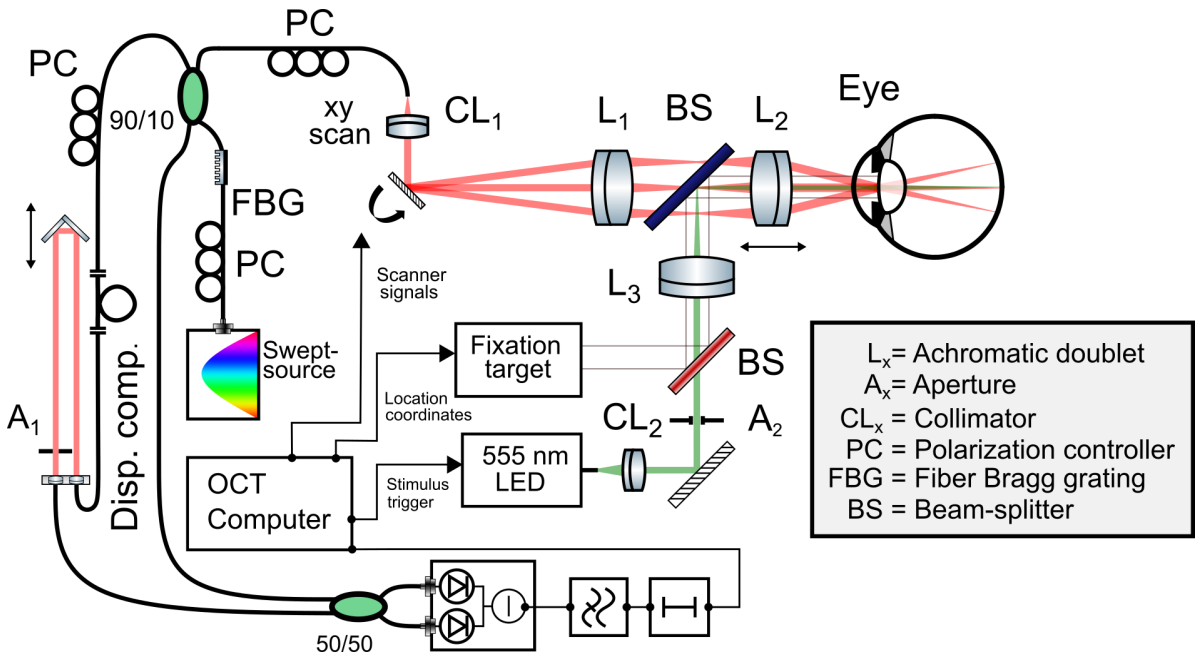

Figure 1. **Schematic of the prototype clinical ORG system**.

2.2 Human subjects

Four subjects were imaged for the present report:

#16: 36-year-old male control subject (36 y.o, male)

#23: 58-year-old female patient whose ophthalmic clinical assessment confirms Stargardt maculopathy, a genetic disorder affecting the macula, with a classical clinical appearance. The condition is observed bilaterally, with minimal peripheral involvement and characterized by a bull's eye appearance. Genetic testing identified a single allele pathogenic variant in the ABCA4 gene (c.4469G>A, p.Cys1490Tyr), consistent with an autosomal recessive pattern. Clinical OCT revealed macular atrophy and parafoveal OS disruption. Humphrey Visual Field (HVF) testing indicates central sensitivity depressions, slightly worse in the right eye. The multifocal electroretinogram (mfERG) shows good central sensitivity in both eyes, while full-field electroretinogram (ffERG) was largely intact.

#27: 75-year-old male patient presenting with vision loss in both eyes. ERG indicates significantly decreased cone function bilaterally, with an unknown etiology. Patient has a history of retinal tears in both eyes, with laser retinopexy repairs. There is a history of posterior vitreous detachment in the left eye without additional complications. The patient is a glaucoma suspect in both eyes, with retinal nerve fiber layer (RNFL) and retinal ganglion cells layer (GCC) thinning.

#28: 61-years-old male subject had retinal dysfunction in both eyes, with uncertain causes, possibly related to anti-retinal antibodies. Genetic testing revealed mutations in CEP250 and CNGA3, but the latter is not considered a manifest cause. Prior skin cancer excision showed squamous cell carcinoma and, but current cancer work-up was negative. Full-field ERG suggests rod bipolar cell and cone function impairment, a missing electronegative (B-wave) waveform, possibly indicating congenital stationary night blindness or anti-N retinal antibodies' impact. The patient denies congenital night blindness and lacks evidence of cancer-associated retinopathy or melanoma-associated retinopathy. The condition seems more like retinal cell dysfunction than progressive degeneration. Objective measurements indicate stable vision despite reported worsening symptoms.

2.3 Imaging protocol

Five minutes of dark adaptation were conducted prior to collecting each set of images. Series of 80 B-scans were collected over 200 ms. After 100 ms, the stimulus flash was presented. In order to facilitate comparison with the control subject, all subjects were imaged at the same locations–in the temporal retina at eccentricities of 2°, 4°, 6°, 8°, and 10°. At each eccentricity, five locations were imaged. These locations lay in an iso-eccentric arc at the given eccentricity, spaced along the arc in such a way that successive stimulus flashes did not overlap. By arranging the locations as such, 25 trials could be acquired with only one round of dark adaptation. Including dark adaptation, the entire session required less than ten minutes, although some time was required prior to imaging to align and instruct the subject and tune the OCT system. All imaging was conducted with approval from the UC Davis IRB and in compliance with the Declaration of Helsinki.

2.4 OCT signal processing

OCT B-scans were processed using well-known methods, previously reported.[15] Acquired spectral fringes were cropped to remove noise near the start and end of the source's sweep. Spectra from single fast scans were averaged to estimate the signal DC, which was subtracted from each spectrum. Chirp in the resultant fringes, due to group velocity dispersion mismatch between sample and reference arms, was removed numerically by manually adjusting the third and second order coefficients in a third order phase polynomial. The optimized phase polynomial was multiplied by each acquired fringe in order to dechirp them. Finally, discrete Fourier transformation (DFT) was used to convert the corrected spectra into B-scans. The B-scans were stored as 128-bit complex-valued arrays.

2.5 Calculation of rate of outer segment length change (v_{OS})

A diagram depicting the data processing method is shown in Fig. 2. It is a modified version of the method described in Vienola et al., 2022.[15] Complex B-scans were registered and aligned vertically using one-dimensional cross-correlation of their axial profiles. The B-scans were then divided into overlapping (or rolling) blocks, numbered $n = 1$ through $n = N$, where N is equal to the total number of B-scans acquired, less the block size. In this report, the block size was three B-scans. Processing a block resulted in a single measurement of v_{OS}, i.e. a single data point in the velocity plots below. B-scans in each block were bulk-motion corrected relative to their first B-scan, using a shifted histogram approach.[16] A semi-automated method was used to segment the IS/OS and COST layers. Investigators identified the approximate location of the IS/OS and COST bands in one block, and similar coordinates were identified in the other blocks automatically, on the basis of their proximity and amplitude. These were visually inspected by the user and adjusted before subsequent processing. The the same coordinates were used for downstream computations on each block, although were permitted to vary among blocks. At each pair of segmented IS/OS and COST coordinates, the phase difference between the two points was calculated, separately for each B-scan. These are expressed as $\Delta\theta_n(x,t)$, where n represents the block index, t represents the time the B-scan was acquired, and x represents the location of the computed phase difference along the fast-scanning dimension. Next, least-squared error linear fitting of unwrapped OCT phase was performed at each x coordinate, with respect to time t. The slope of the phase, or phase velocity, $(v_{OS,n}(x))$ contains a record of the rate of OS length change for many locations along the x (fast scanning) dimension of the block. These phase velocities were then averaged along that dimension to produce each block's rate of OS length change, $v_{OS,n}$.

2.6 Quantification of ORG responses

Responses from each of the five locations at each eccentricity were averaged, and this mean response was used for further analysis. We sought to quantify the ORG responses and applied two previously proposed[15] metrics, meant to capture the amplitude of the ORG response. v_{min} is defined as the most negative velocity observed after the flash onset, and v_{20-40} is the average velocity between 20 ms to 40 ms post-flash. These values were calculated from the averaged responses at each eccentricity in each subject. Finally, the values derived from the patient measurements were normalized by dividing them by the control subject's values in order to permit rapid visual assessment of the patient responses.

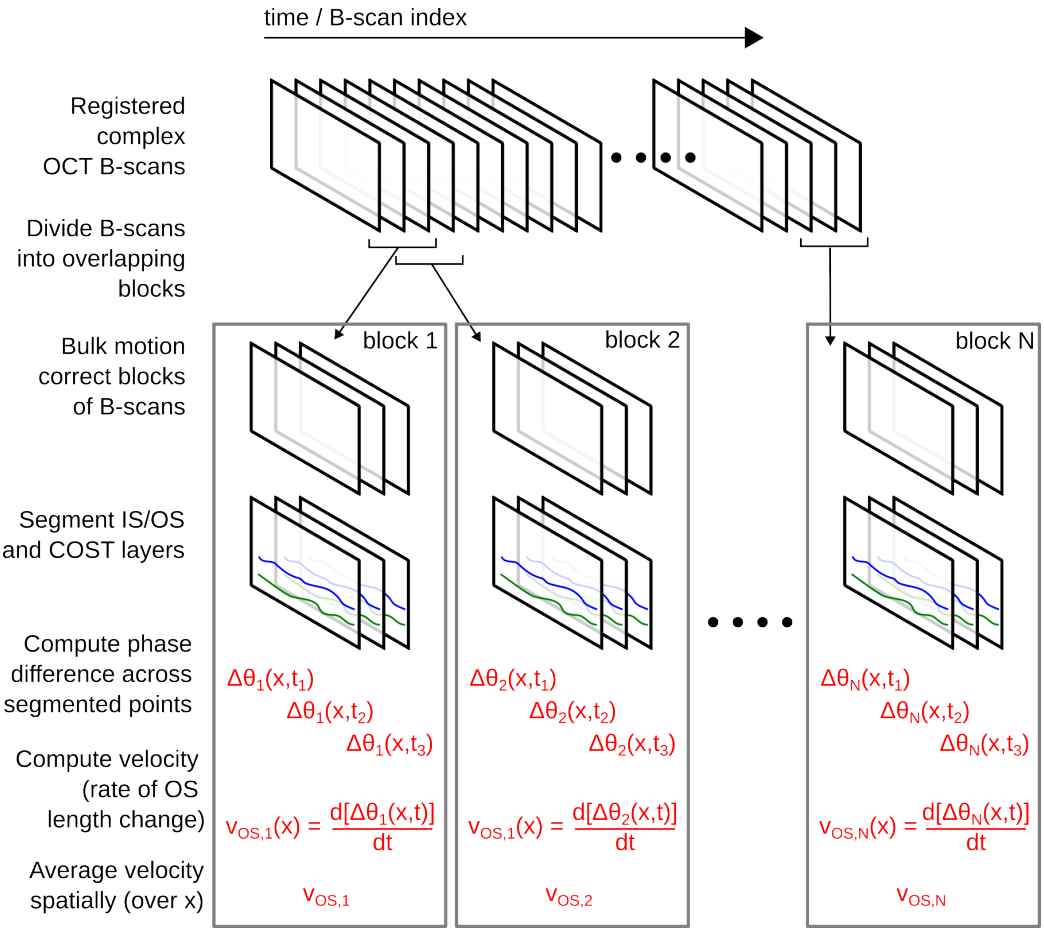

Figure 2. **Velocity-based ORG data processing steps**. Complex B-scans were aligned and divided into overlapping blocks of three. B-scans in each block were bulk-motion corrected and the IS/OS and COST layers were segmented. In each B-scan, at each pair of segmented IS/OS and COST coordinates, the phase difference was calculated: $\Delta\theta_n(x,t)$, where n, t, and x represent the block index, time, and location along the fast-scanning dimension. Next the slope of the phase was determined at each x coordinate, resulting in $v_{OS,n}(x)$. These phase velocities were then averaged spatially to produce each block's rate of OS length change, $v_{OS,n}$.

3. RESULTS

3.1 Images and ORG responses

B-scans from all subjects at all eccentricities exhibited visible IS/OS and COST bands. These were successfully segmented using the semi-automated procedure described above. Representative B-scans from two subjects (#16 and #27) are shown in Fig. 3. The points from the highlighted location were used for ORG computations. The points used for ORG calculations are plotted. The lateral extent of the ORG analysis region was determined by the width of the 1.2° stimulus flash, which did not cover the entire 2.5° imaged region.

The velocity ORG response, v_{OS} was calculated at each of the 25 locations imaged in each subject–five iso-eccentric patches at each of five eccentricities. All responses from the control subject (#16) were similar to previously reported measurements.[15] We observed a strong association between eccentricity and v_{min}, and a slightly weaker association between v_{20-40} and eccentricity. Representative responses from the 2° and 4° measurements in the control subject (#16) are shown in Fig. 4(left). Most of the responses from patients differed qualitatively from the control subject. Some had attenuated early contractions and others had attenuated or missing elongation phases. Example responses from a patient with unexplained vision loss (#27) are shown in Fig. 4(right), from the same eccentricities. The early OS contraction in the patient has smaller amplitude, and

the elongation appears to be attenuated as well. OS contraction was evident in all trials for all subjects over the first ∼15 ms. Elongation was observed in some trials over the following ∼50 ms. Velocities after ∼70 ms exhibited substantial noise and inter-trial variability, hypothetically attributed to reflexive eye movements after the flash, which resulted in phase noise that could not be corrected numerically.

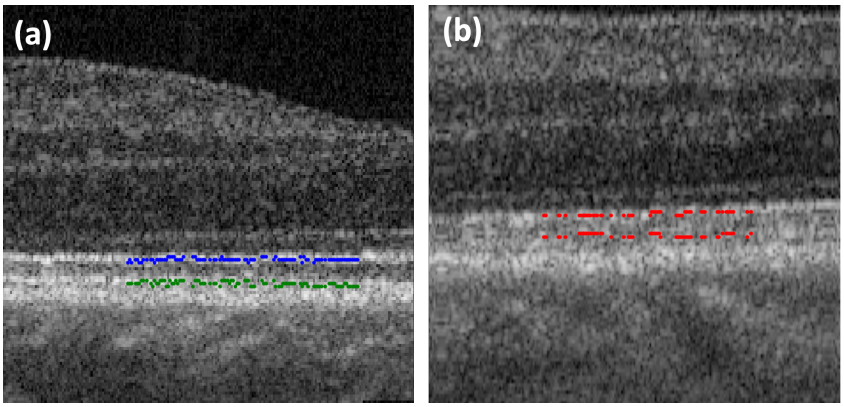

Figure 3. **Representative B-scans from ORG measurement**. (a) and (b) are B-scan images of control subject (#16) and patient (#27) at 2°. The ORG responses were computed from the points highlighted in the IS/OS and COST bands.

3.2 ORG metrics

After quantifying ORG responses using v_{min} and v_{20-40}, and normalizing the patient values to the control values, were able to visualize some general trends. Two of the patients, #27 and #28, exhibited similar values for v_{min} to those observed in the control subject, at eccentricities of 2° to 4°, but one of the patients, #23, exhibited significantly lower contraction amplitude at all eccentricities. These results can be seen in Fig. 5(a,c).

Most patient measurements exhibited significantly lower values of v_{20-40}, compared to the control subject. The exceptions were the 2° and 6° measurements taken from patient #28, which were similar to or greater than the responses from the control subject. These results can be seen in Fig. 5(b,d).

3.3 Discussion

Little is known about the physiological origins of the ORG response, but some hypotheses have been proposed. The elongation phase has been hypothesized to originate from phototransduction-related changes in intracellular osmolyte concentrations, and subsequent movement of water into the cell. Zhang *et al.* studied light-evoked changes in the amplitude of the OCT signal in the mouse, as well as the role of transducin in light-evoked swelling of the mouse outer segment.[13] They showed reproducible light-evoked elongation of the OS, which was suppressed in the transducin knockout. This suggests that the elongation of the OS is a consequence of phototransduction, downstream of the activation of transducin by activated opsin. This hypothesis is further bolstered by the recent report that patients with retinitis pigmentosa (RP) exhibit weaker ORG responses.[10] Those investigators used principal component analysis (PCA) on concatenated responses to chromatic stimuli and reported a reduction of the Euclidean distance of the first two principal components from zero. Their study included two patients without genetic testing and one with an USH2A mutation, whose precise role in RP development is unknown. As such, little can be said about how exactly the phototransduction pathway was affected. Nevertheless, the study provides some evidence that alterations in the pathway could cause changes in the elongation component of the ORG response.

In AO-ORG studies,[3,4] the highest rate of OS elongation appeared to occur between 20 ms to 40 ms post-stimulus. Moreover, in our earlier investigation of the present velocity-based ORG method, we observed that positive values of v_{OS} were most reliably found in the same interval. As such, we believe that the v_{20-40} ORG metric should reflect the rate of elongation. While not discussed directly, it is evident from other studies that

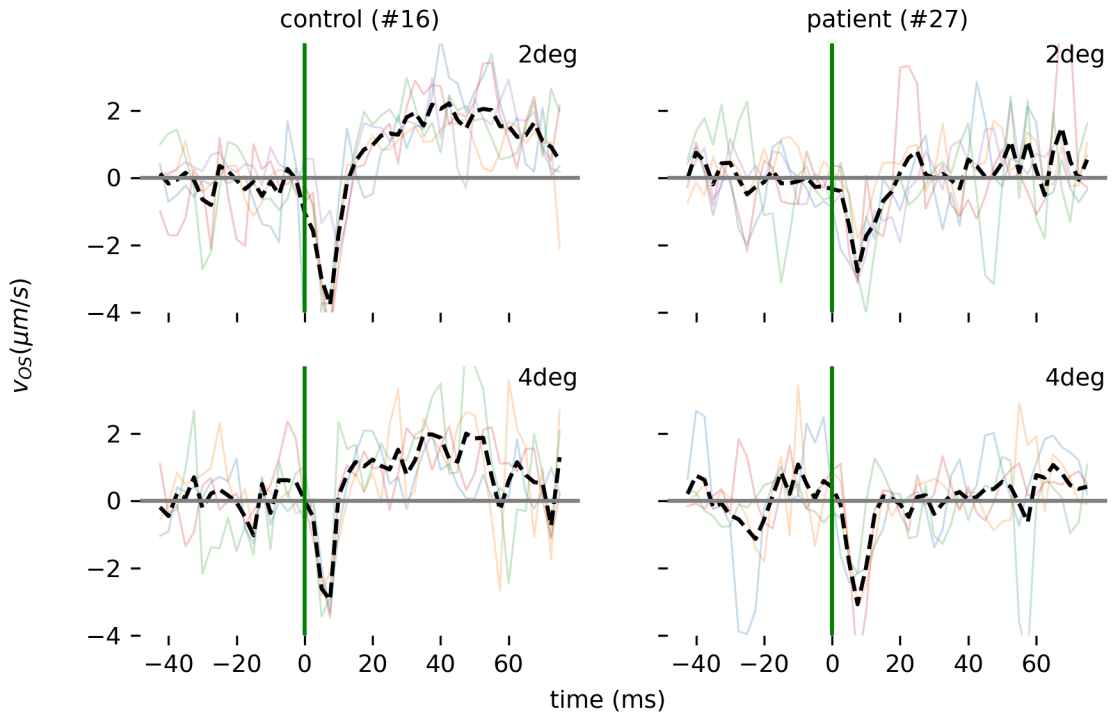

Figure 4. **Representative ORG responses from control and patient measurements**. Control responses are on the left; patient responses are on the right. Responses from 2 deg are on top, and responses from 4 deg are on bottom. Vertical solid green line indicates time of stimulus onset. Horizontal solid gray line indicates zero velocity, i.e., no response. Dashed black lines represent the averaged response from up to five iso-eccentric regions, with the individual responses plotted faintly in solid colors. The control subject exhibited characteristic features at all eccentricities: v_{OS} was negative between the flash and 20 ms and positive thereafter for 20 ms to 40 ms. These suggest an initial fast contraction of the OS followed by a slower elongation. All subjects exhibited early contraction at 2° and 4°, some with attenuated amplitudes.

the rate of OS elongation is related to the maximum OS length.[5,6] In our study of the rod ORG, we found that the rate of elongation was more closely associated with stimulus dose than the maximum excursion of the OS.[9]

The early contraction of the OS has been hypothetically attributed to the early receptor potential (ERP).[7] The ERP is due to a photoisomerization-related change in the dipole moment of opsins. This has been hypothesized to cause an increase in intermolecular repulsion among opsins and an associated increase in the OS disc diameter and contraction of the OS length. Under this hypothesis, changes in the early contractile stage of the ORG response would indicate either depletion of unactivated photopigment or ultrastructural alterations in the OS discs that interfere with the normal electrostatic effects.

Disease-related changes in v_{20-40} are by themselves non-specific, as upstream abnormalities (e.g., in photopigment availability) would affect it. Patient #23, for example, who has Stargardt maculopathy with a pathogenic mutation in ABCA4, appears to have attenuation of both ORG components at most locations. Her v_{20-40} values are significantly lower than the control subject's at all eccentricities (see Fig. 5(d)). However it would be incorrect to assume that this indicates a phototransduction failure because we also observed attenuated v_{min} at most locations, as low as 33% of normal at 2 deg and 54% of normal at 4 deg (Fig. 5(c)). Assuming that the ERP drives v_{min}, we can infer that her opsins are not absorbing as many photons as we would expect. This could be due to any number of factors–visual cycle defects, outer segment structural flaws, or even prereceptoral factors such as media opacity or cataract (although those were ruled out clinically). Reductions in pigment density have been reported in Stargardt's patients,[17] presumed to be due to a hampered visual cycle. However, accumulations of lipofuscin in the RPE are also a consequence of the ABCA4 mutation, and these can lead to

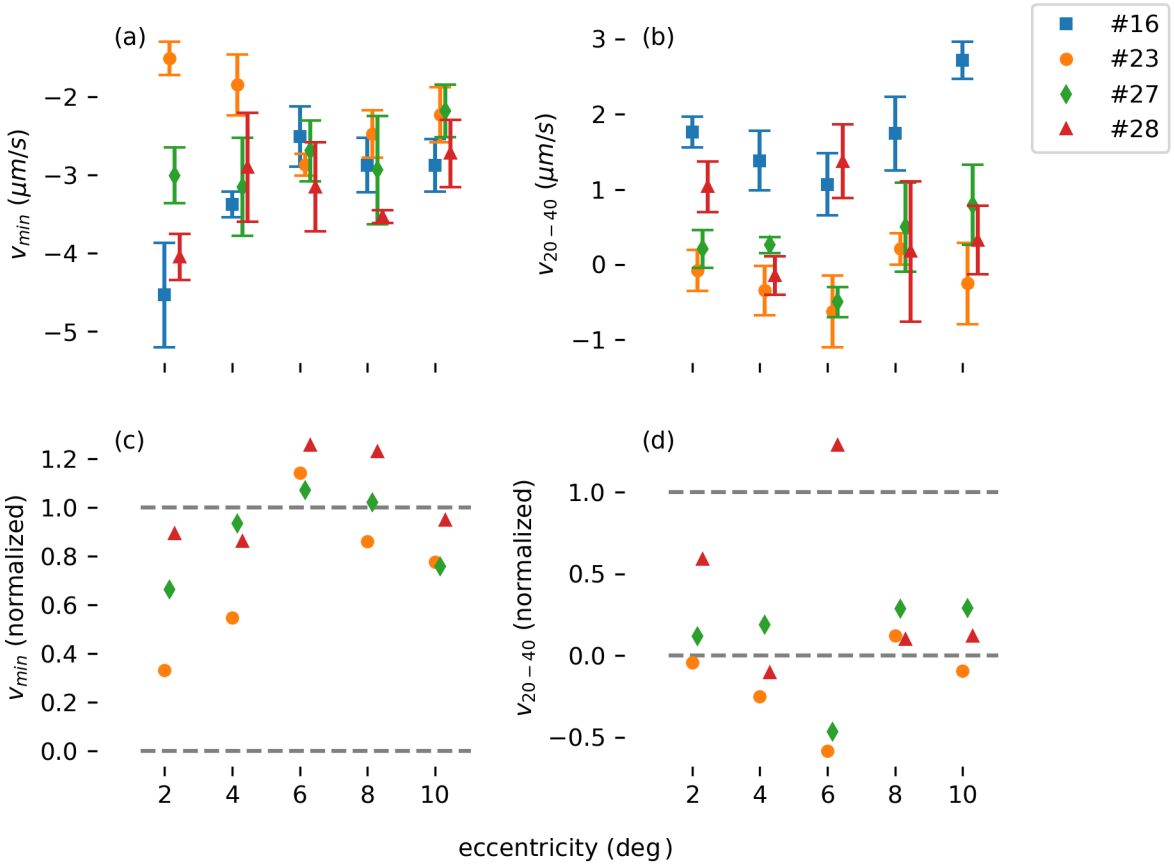

Figure 5. **Comparison of ORG metrics of all subjects from** 2°, 4°, 6°, 8°, **and** 10°. (a) The highest contraction (v_{min}) of the OS within 20 ms after applying the applied external stimulus, (c) which is normalized with control subjects v_{min}. (b) post stimulus OS elongation (v_{20-40}) and (d) normalized post stimulus OS elongation at different eccentricities for different subjects.

reduction in RPE phagocytosis of photoreceptor OS and other general problems in photoreceptor homeostasis. It is interesting to note that the abnormal ORG findings are consistent with the patient's subjective tests, but that neither ERG nor mfERG detected any abnormalities. The spatial resolution of the mfERG (∼1 deg) is similar to ours (1.2 deg), which is of special interest. This could be due to noise or error in one or both modalities, but if not it suggests adaptation of the cones to subnormal pigment isomerization and early phototransduction, possibly through modulation of phototransduction gain.

Unlike the case of attenuated v_{min} and v_{20-40}, the combination of a normal v_{min} with an absent or attenuated v_{20-40} leads to a narrower hypothetical picture. This is the case in patients #27 and #28, both of whom presented with unexplained vision loss. In these two patients, v_{min} was above 60% of normal at all eccentricities, and above 85% of normal at most. Example responses from #27 can be seen in Fig. 4, where the contraction can be seen clearly while the elongation appears to be highly attenuated or absent at most locations. Patient #28 exhibited values of v_{20-40} 60% and 130% of normal at 2 deg and 6 deg, but attenuated values at the three other eccentricities. Patient #27 exhibited attenuated values at all eccentricities. The values of v_{min} and v_{20-40}, normalized to the control subject, can be seen in Fig. 5(c,d). Genetic testing has not yet been performed on #27, and while it has on #28, the mutations revealed were not clinically thought to be relevant to his vision loss. In the case of patient #27, ophthalmic clinical assessment confirmed vision loss in both eyes, and the ERG

response showed a significantly lower response in both eyes. For subject #28, full-field ERG suggests rod bipolar cell and cone function impairment, a missing electronegative (B-wave) waveform. The cause of vision loss in both patients is unknown.

The results presented here are a demonstration of the proto-clinical velocity-based ORG method's capability to measure ORG responses in patients with vision loss and its potential role in disease diagnosis or staging. However, this work could be improved in a number of ways:

1. We compared patient ORG responses to just one control subject's. We plan to build a database of normative responses to give us a better sense of normal variability and the ability to decide if deviations in patient responses are statistically significant. Ideally we would be able to compare the responses of patients to those of age-matched controls, as we have informally observed age effects in our measurements. We plan to initiate collection of this data soon, but did not want to begin until the experimental protocol is finalized.

2. We have not fully explored the ORG processing pipeline (Fig. 2). The acquired data are rich and we may be overlooking ways to improve the SNR of the acquired signals. For instance, during the initial stages of aligning B-scans and numerically correcting bulk motion, we may be able to make inferences about the stability of the retina, and use these to filter the computed values of v_{OS}.

3. We have striven to make the test as short and easy as possible for patients, which has thus far precluded us from acquiring more than one or two rounds of measurement (at all locations) for each patient. If the time required by a single trial could be shortened, we would be able to acquire more than two trials, and average these together to improve the SNR of the test. Other groups have used shorter dark adaptation times,[5] and we plan to test this method using 90 seconds of dark adaptation rather than five minutes.

4. We imaged many patients whose results are not presented here. Some patients (e.g., advanced RP and geographic atrophy) did not possess enough intact retinal structure to segment the IS/OS and COST and calculate a response. The method presented here is quantitative and based on a physical model of the OS, and the resulting measurements can be compared with other ORG approaches. However, we are exploring alternative, statistical methods–more akin to angiographic methods–that might permit gross measurements of response even in the absence of clear retinal bands.

5. In an effort to make the test quick for patients, and also to facilitate comparison with normal responses, we elected to image the patients at the same locations as the control subject. This approach neglects the context offered by wider-field imaging of atrophy or morphological changes caused by disease (with our instrument or in the clinic). An alternative approach would be to select regions of interest in the patients' retinae, e.g., in transitional zones between healthy and atrophic retina or near pseudodrusen and drusen.

6. Patients have tended to fatigue quickly. The task of sitting and fixating on a fixation target can be very challenging, and regardless of their motivation to volunteer and help, they sometimes become fatigued. We will continue to explore methods to make the test quicker and easier.

4. CONCLUSION

We have tested the proto-clinical, velocity-based ORG on subjects affected by disease and successfully measured ORG responses from individuals with vision loss. Furthermore, distinct components of the ORG response appeared to be affected in visually impaired patients. Future work includes development of a normative database, including individuals of all ages, and improvements in the imaging protocol and data processing pipeline.

ACKNOWLEDGMENTS

We would like to thank: Susan Garcia (UC Davis) for her efforts in patient coordination; Profs. John S. Werner, Paul A. Sieving, and Glenn Yiu (UC Davis) for helpful discussions about photoreceptor function and disease; Prof. Yifan Jian (OHSU) for development of OCT acquisition software; NIH grants R00-EY-026068, R01-EY-033532, R01-EY-031098, R01-EY-26556, and P30-EY-012576.

REFERENCES

[1] Choma, M. A., Ellerbee, A. K., Yang, C., Creazzo, T. L., and Izatt, J. A., "Spectral-Domain Phase Microscopy," *Optics Letters* **30**(10), 1162–1164 (2005).

[2] Jonnal, R. S., Rha, J., Zhang, Y., Cense, B., Gao, W., and Miller, D. T., "In Vivo Functional Imaging of Human Cone Photoreceptors," *Optics Express* **15**(24), 16141–16160 (2007).

[3] Hillmann, D., Spahr, H., Pfäffle, C., Sudkamp, H., Franke, G., and Hüttmann, G., "In Vivo Optical Imaging of Physiological Responses to Photostimulation in Human Photoreceptors," *Proceedings of the National Academy of Sciences of the United States of America* **113**, 13138–13143 (Nov. 2016).

[4] Azimipour, M., Migacz, J. V., Zawadzki, R. J., Werner, J. S., and Jonnal, R. S., "Functional Retinal Imaging Using Adaptive Optics Swept-Source OCT at 1.6 MHz," *Optica* **6**(3), 300–303 (2019).

[5] Zhang, F., Kurokawa, K., Lassoued, A., Crowell, J. A., and Miller, D. T., "Cone Photoreceptor Classification in the Living Human Eye from Photostimulation-Induced Phase Dynamics," *Proceedings of the National Academy of Sciences* **116**(16), 7951–7956 (2019).

[6] Pandiyan, V. P., Maloney-Bertelli, A., Kuchenbecker, J. A., Boyle, K. C., Ling, T., Chen, Z. C., Park, B. H., Roorda, A., Palanker, D., and Sabesan, R., "The Optoretinogram Reveals the Primary Steps of Phototransduction in the Living Human Eye," *Science Advances* **6**, eabc1124 (Sept. 2020).

[7] Boyle, K. C., Chen, Z. C., Ling, T., Pandiyan, V. P., Kuchenbecker, J., Sabesan, R., and Palanker, D., "Mechanisms of Light-Induced Deformations in Photoreceptors," *Biophysical Journal* **119**, 1481–1488 (Oct. 2020).

[8] Liu, Z., Zhang, F., Zucca, K., Agrawal, A., and Hammer, D. X., "Ultrahigh-speed multimodal adaptive optics system for microscopic structural and functional imaging of the human retina," *Biomedical Optics Express* **13**, 5860–5878 (Nov. 2022).

[9] Azimipour, M., Valente, D., Vienola, K. V., Werner, J. S., Zawadzki, R. J., Zawadzki, R. J., and Jonnal, R. S., "Optoretinogram: Optical Measurement of Human Cone and Rod Photoreceptor Responses to Light," *Optics Letters* **45**, 4658–4661 (Sept. 2020).

[10] Lassoued, A., Zhang, F., Kurokawa, K., Liu, Y., Bernucci, M. T., Crowell, J. A., and Miller, D. T., "Cone photoreceptor dysfunction in retinitis pigmentosa revealed by optoretinography," *Proceedings of the National Academy of Sciences* **118**, e2107444118 (Nov. 2021).

[11] Bizheva, K., Pflug, R., Hermann, B., Považay, B., Sattmann, H., Qiu, P., Anger, E., Reitsamer, H., Popov, S., Taylor, JR., et al., "Optophysiology: Depth-Resolved Probing of Retinal Physiology with Functional Ultrahigh-Resolution Optical Coherence Tomography," *Proceedings of the National Academy of Sciences-USA* **103**(13), 5066–5071 (2006).

[12] Srinivasan, V. J., Wojtkowski, M., Fujimoto, J. G., and Duker, J. S., "In vivo measurement of retinal physiology with high-speed ultrahigh-resolution optical coherence tomography," *Optics Letters* **31**, 2308–2310 (Aug. 2006).

[13] Zhang, P., Zawadzki, R. J., Goswami, M., Nguyen, P. T., Yarov-Yarovoy, V., Burns, M. E., and Pugh, E. N., "In Vivo Optophysiology Reveals That G-Protein Activation Triggers Osmotic Swelling and Increased Light Scattering of Rod Photoreceptors," *Proceedings of the National Academy of Sciences* **114**(14), E2937–E2946 (2017).

[14] Srinivasan, V. J., Chen, Y., Duker, J. S., and Fujimoto, J. G., "In Vivo Functional Imaging of Intrinsic Scattering Changes in the Human Retina with High-Speed Ultrahigh Resolution OCT.," *Optics Express* (2008).

[15] Vienola, K. V., Valente, D., Zawadzki, R. J., Zawadzki, R. J., and Jonnal, R. S., "Velocity-based optoretinography for clinical applications," *Optica* **9**, 1100–1108 (Oct. 2022).

[16] Makita, S., Hong, Y., Yamanari, M., Yatagai, T., and Yasuno, Y., "Optical Coherence Angiography," *Optics Express* **14**(17), 7821–7840 (2006).

[17] van Meel, G. J. and van Norren, D., "Foveal densitometry as a diagnostic technique in stargardt's disease," *American journal of ophthalmology* **102**(3), 353–362 (1986).